Articles

Temperature Dependence of the Vibration-Vibration Energy Transfer for $HF(v=n)+H_2(v=0)$ and $DF(v=n)+D_2(v=0)$

Chang Soon Lee* and Yoo Hang Kim†

Department of Chemistry, Changwon National University, Changwon 641-773
†Department of Chemistry, Inha University, Inchon 402-751. *Received August 30, 1991*

Vibration-to-vibration energy transfer probabilities for $HF(v=n)+H_2(v=0)\rightarrow HF(v=n-1)+H_2(v=1)$ and $DF(v=n)+D_2(v=0)\rightarrow DF(v=n-1)+D_2(v=1)$ including both the vibration-to-vibration and translation ($V-V$, T) and vibration-to-vibration and rotation ($V-V$, R) energy transfer paths have been calculated semiclassically using a simplified collision model and Morse-type intermolecular interaction potential. The caculated results are in reasonably good agreement with those obtained by experimental studies. They also show that the transition processes for $HF(v=1-3)+H_2(v=0)\rightarrow HF(v=0-2)+H_2(v=1)$ and $DF(v=1, 4)+D_2(v=0)\rightarrow DF(v=0, 3)+D_2(v=1)$ are strongly dependent on the $V-V$, T path at low temperature but occur predominantly *via* the $V-V$, R path with rising temperature. The vibration-to-vibration energy transfer for $HF(v=4)+H_2(v=0)\rightarrow HF(v=3)+H_2(v=1)$ and $DF(v=2-3)+D_2(v=0)\rightarrow DF(v=1-2)+D_2(v=1)$ occur predominantly *via* $V-V$, R path and $V-V$, T path through whole temperatures, respectively.

Introduction

In recent years the vibration-to-vibration ($V-V$) energy transfer of hydrogen halides or of deuterium halides have been studied with various collision partners.[1-6] These studies have been recognized important because of the great interest in theories used to predict the $V-V$ energy transfer and in the development of hydrogen halide chemical lasers.

In these collision systems the $V-V$ energy transfer processes for $HF(v=n)$ and $DF(v=n)$ with the homonuclear diatomic molecules can be expressed as follows;

$$HF(v=n)+X_2(v=0)\rightarrow HF(v=n-1)+X_2(v=1)+\Delta E$$

$$DF(v=n)+X_2(v=0)\rightarrow DF(v=n-1)+X_2(v=1)+\Delta E$$

where X represents H, D, N, O, etc. This process is either endothermic or exothermic reaction according to the sign of the energy mismatch ΔE. In case of the endothermic process (*i.e.*, $\Delta E<0$), energy mismatch ΔE will have to be transferred to the vibrational motion of the ground state molecule from the translational or rotational motion. Conversely, in the exothermic one (*i.e.*, $\Delta E>0$), ΔE will be transferred to the translational or rotational motion. The $V-V$ energy transfer processes of these two reactions thus can be accomplished via both the vibration to vibration and translation ($V-V$, T), and the vibration to vibration and rotation ($V-V$, R) mechanisms, which can be two possible pathways for the supply or removal of the energy mismatch.

In our previous papers the $V-V$, T energy transfer of hydrogen chlorides[7] and of hydrogen bromides[8] was described by the long-lived collision model which had been recently developed to take into account the relatively weak hydrogen bonding between these molecules. And the combination of long-lived collision model and the $V-V$, R energy transfer model can satisfactorily account for the vibrational relaxation probabilities for $V-V$ energy transfer of $NO(v=2)$ by $NO(v=0)$[9].

In this paper, it will be shown that both the long-lived collision model, which considers the local translational mode due to the binding energy of weakly bound complex between hydrogen fluoride and nonpolar molecule[10], and the $V-V$, R energy transfer model can be applied to the calculation of the $V-V$ energy transfer probabilities for the above processes. As illustrative examples, the following two processes are chosen;

$$HF(v=n)+H_2(v=0)\rightarrow HF(v=n-1)+H_2(v=1)+\Delta E \quad \text{(a)}$$

$$DF(v=n)+D_2(v=0)\rightarrow DF(v=n-1)+D_2(v=1)+\Delta E \quad \text{(b)}$$

Furthermore, we wish to find out the effect of temperature, vibrational quantum number and energy mismatch on the energy transfer probabilities. Also, the results will be compared with those obtained from other $V-V$ energy transfer experiments[11-22].

The collision model and the derivation of the equation for the energy transfer probability for $V-V$, T and $V-V$, R are given elsewhere[7-9,23]. Those expressions are summarized briefly in the next sections.

$V-V$, T Energy Transfer

The interaction potential is assumed to be of Morse type;

$$U(r)=D\left[\exp\left(\frac{r_e-r}{a}\right)-2\exp\left(\frac{r_e-r}{2a}\right)\right] \quad (1)$$

where r is the distance between H (or D) atom of HF (or DF) molecule and H (or D) atom of H_2 (or D_2) molecule, r_e, its equilibrium value, and D and a, potential parameters to be determined. When the relative separation, R, between the colliding molecules is significantly greater than the equilibrium bond diatance d_1 and d_2, the atom-atom distance can be approximated as $r\simeq R-\gamma(d_1+x_1)\cos\theta_1+\frac{1}{2}(d_2+x_2)\cos\theta_2$. Subscripts 1 and 2 represent HF (or DF) molecule and H_2 (or D_2), molecule, respectively; θ_i the angle between molecular axes and R, x_i the vibrational coordinate, and γ

$=m_F/(m_H+m_F)$ or $m_F/(m_D+m_F)$. Substituting this distance into Eq. (1), the overall interaction potential could be expressed as follows,

$$U(R,\ \theta_1,\ \theta_2,\ x_1,\ x_2)=U_o(R,\ \theta_1,\ \theta_2)+x_1\frac{\partial U}{\partial x_1}+x_2\frac{\partial U}{\partial x_2}+x_1x_2\frac{\partial^2 U}{\partial x_1\partial x_2}+\cdots \quad (2)$$

We shall replace x_i by $(\hbar/2M_i\omega_i)(\mathbf{a}_i^{+}+\mathbf{a}_i)$, where $\mathbf{a}_i^{+}$ and $\mathbf{a}_i$ are ladder operators, and M_i and ω_i are the reduced mass and angular frequency of the ith oscillator, respectively.

After including the averaging effect of the rotational motions of the colliding molecules, the orientation-averaged potential with the new equilibrium distance R_e^* can be written as;

$$\bar{U}_o(R)=(2\pi)^{-2}\int_o^{2\pi}\int_o^{2\pi}U_o(R,\ \theta_1,\ \theta_2)x_1x_2\,d\theta_1\,d\theta_2$$

$$=D^*\left[\exp\left(\frac{R_e^*-R}{a}\right)-2\exp\left(\frac{R_e^*-R}{2a}\right)\right] \quad (3)$$

where, $D^*=\dfrac{D\left[I_o\left(\frac{1}{2}Q_1\right)I_o\left(\frac{1}{2}Q_2\right)\right]^2}{[I_o(Q_1)\,I_o(Q_2)]}$

I_i is the modified Bessel function of order i, and Q_1 and Q_2, are d_1/a and $d_2/2a$ respectively.

From Eqs. (1) and (2),

$$\bar{U}_{12}(R,\ x_1,\ x_2)=(2\pi)^{-2}\int_o^{2\pi}\int_o^{2\pi}\frac{\partial^2 U}{\partial x_1\partial x_2}x_1x_2\,d\theta_1\,d\theta_2$$

$$=\frac{D^*\gamma\hbar}{4a^2(M_1M_2\omega_1\omega_2)^{1/2}}\left[K_1\exp\left\{\frac{R_e^*-R(t)}{a}\right\}-\frac{1}{2}K_2\exp\left\{\frac{R_e^*-R(t)}{2a}\right\}\right](a_1^{+}+a_1)(a_2^{+}+a_2)$$

$$=F(t)\ (a_1^{+}+a_1)(a_2^{+}+a_2) \quad (4)$$

where $K_1=I_1(Q_1)\,I_1(Q_2)/I_o(Q_1)I_o(Q_2)$ and $K_2=I_1\left(\frac{1}{2}Q_1\right)I_1\left(\frac{1}{2}Q_2\right)/2I_o\left(\frac{1}{2}Q_1\right)I_o\left(\frac{1}{2}Q_2\right)$. In the vicinity of R_e^*, the collision trajectory has been shown to be[7] $R(t)=R_e^*-2a(E/D)^{1/2}\cos[(D^*/2\mu)^{1/2}(t/a)]$, where E is initial collision energy and μ is the reduced mass of the collision system.

For $v-1,\ 1\rightarrow v,\ 0$ transition, the transition probability can be wtitten in the form of

$$P_{v-1,\ 1}^{v,\ 0}(E)=v\sin^2[\hbar^{-1}\int_{-\infty}^{\infty}F(t)\exp(i\,\Delta\omega t)dt]\cos^{2(v-1)}[\hbar^{-1}\int_{-\infty}^{\infty}F(t)\exp(i\Delta\omega t)dt] \quad (5)$$

where $\Delta\omega=\Delta E/\hbar$. The integral in Eq. (5) with the time dependence determined by the collision trajectory can be written as;

$$\hbar^{-1}\int_{-\infty}^{\infty}F(t)\exp(i\Delta\omega t)\,dt=\frac{\gamma D^*}{4a^2(M_1M_2\omega_1\omega_2)^{1/2}}\left[2\pi a(2\mu/D)^{1/2}\times\left\{\frac{K_1}{2\pi}\int_{\phi_1}^{\phi_2}(\cos n\phi+i\sin n\phi)\exp[2(E/D^*)^{1/2}\cos\phi]d\phi-\frac{K_2}{2\pi}\int_{\phi_1}^{\phi_2}(\cos n\phi+i\sin n\phi)\exp[(E/D^*)^{1/2}\cos\phi]d\phi\right\}\right. \quad (6)$$

Noting that, from the collision trajectory, the period T of the local translational motion is $2\pi a(2\mu/D^*)^{1/2}$, the integration limits $(\phi_1,\ \phi_2)$ can be replaced by $(-T/2,\ T/2)$, which corresponds to $(-\pi,\ \pi)$. Then, the result becomes;

$$\hbar^{-1}\int_{-\infty}^{\infty}F(t)\exp(i\Delta\omega t)dt=\frac{\gamma D^*}{4a^2(M_1M_2\omega_1\omega_2)^{1/2}}\{2\pi a(2\mu/D^*)^{1/2}[K_1I_n(2z)-K_2I_n(z)]\} \quad (7)$$

where $z=(E/D^*)^{1/2}$ and the order of the Bessel functions appearing in the last bracket is $n=\Delta\omega a(2\mu/D^*)^{1/2}$. E in the energy exchange probability expression should be replaced by the symmetrized energy $\frac{1}{4}\{[E(1-b^2/r^{*2})]^{1/2}+[E(1-b^2/r^{*2})+\Delta E]^{\frac{1}{2}}\}^2$ considering the effect of the non-zero impact parameter(b) collisions. Here r^* is the hard-sphere collision diameter. With this consideration into account, the thermal-averaged probability can be written as,

$$P_{v-1,\ 1}^{v,\ 0}(T)=\frac{1}{(kT)^2\pi r^{*2}}\int_o^{r^*}\int_o^{D^*}2\pi b\,EP_{v-1,\ 1}^{v,\ 0}(E,\ b)\exp(-E/kT)\,dE\,db \quad (8)$$

V−V, R Energy Transfer

The energy difference due to the vibrational mismatch in the $V-V$ processes $HF(v=n)+H_2(v=0)$ and $DF(v=n)+D_2(v=0)$, ΔE, can also be removed by the rotational motion of H_2 (or D_2) molecule[24]. In the region of the closest distance of approach R_o, the rotation of HF (or DF) molecule can be replaced by its average effect;

$$\bar{U}_{12}(\theta_2)=(2\pi)^{-1}\int_o^{2\pi}\frac{\partial^2 U}{\partial x_1\partial x_2}x_1x_2\,d\theta_1$$

$$=\frac{D^*\gamma\hbar}{4a^2(M_1M_2\omega_1\omega_2)^{1/2}}\left\{K_3\exp\left(\frac{R_e^*-R_o}{a}\right)\exp(-Q_2\cos\theta_2)-K_4\exp\left(\frac{R_e^*-R_o}{2a}\right)\exp\left(-\frac{1}{2}Q_2\cos\theta_2\right)\times\cos\theta_2(a_1^{+}+a_1)(a_2^{+}+a_2)\right. \quad (9)$$

where $K_3=I_1(Q_1)/I_o(Q_1)I_o(Q_2)$ and $K_4=I_1\left(\frac{1}{2}Q_1\right)/2I_o\left(\frac{1}{2}Q_1\right)I_o\left(\frac{1}{2}Q_2\right)$. Assuming that the translational motion is frozen in the vicinity of R_o during removal of ΔE by rotation, the time dependence is solely due to the rotational trajectory $\theta_2(t)$. In the region of strong interaction where $\theta_2\simeq\pi$, $\cos\theta_2$ is not significanly different from -1, thus $\cos\theta_2$ in the pre-exponential part is replaced by -1, but not so in the exponent. In this region, the rotational trajectory has been found to be[25]

$$\exp\left(-\frac{1}{2}Q_2\cos\theta_2\right)=\frac{\alpha_o}{i}(2I/A)^{1/2}(t-i\tau)^{-1} \quad (10)$$

where $A=[D^*/I_o(Q_2)]\exp\left(\frac{R_e^*-R_o}{a}\right)$,

$$B=\left[2D/I_o\left(\frac{1}{2}Q_2\right)\right]\exp\left(\frac{R_e^*-R_o}{2a}\right),$$

$$\tau=\left(\frac{1}{2}I\pi\right)^{1/2}\sum_{i=o}^{\infty}\frac{\Gamma\left(\frac{1}{2}+i\right)\alpha_i}{\Gamma(1+i)E_r^{1/2+i}},$$

$$\alpha_o=\frac{1+\alpha}{Q_2};\ \alpha_{1/2}=-\frac{\alpha_o}{2A^{1/2}}\left(B+\frac{\beta}{1+\alpha}\right),$$

$$\alpha_1=\frac{\alpha_o(2B\beta+\delta)}{2A(1+\alpha)};\ \alpha=\frac{9}{2Q_2^2}\left(1+\frac{4}{3Q_2^2}\right);$$

$$\beta=\frac{22}{Q_2^2}\left(1+\frac{24}{11Q_2^2}\right)A;\ \delta=\frac{34}{Q_2^2}\left(1+\frac{72}{17Q_2^2}\right)A^2,$$

and I is the moment of inertia.

From Eqs. (9) and (10), with the contour integration

$$\int_{-\infty}^{\infty}\frac{\exp(i\Delta\omega t)}{(t-i\tau)^n}\,dt=[2\pi(i\Delta\omega)^n/\Delta\omega\Gamma(n)]\exp(-\Delta\omega\tau),$$

we find

$$\hbar^{-1}\int_{-\infty}^{\infty}F(t)\ \exp(i\,\Delta\omega\,t)\,dt=\frac{\pi\gamma\Delta\omega\alpha_o^2 I}{a^2(M_1M_2\omega_1\omega_2)^{1/2}}\ \frac{I_1(Q_2)}{I_o(Q_1)}$$

$$\left\{1-\frac{I_1\left(\frac{1}{2}Q_1\right)}{2I_1(Q_1)}\times\left[\frac{D^*I_o(Q_1)}{2I}\right]^{1/2}\frac{1}{\Delta\omega\alpha_o}\right\}\exp(-\Delta\omega t)\quad(11)$$

The dependence of the energy transfer probability on temperature could be obtained by averaging $P^{v,o}_{v-1,\,1}(E_r,\,E)$ over the distributions of initial collision energy, and along with average over impact parameter (b);

$$P^{v,o}_{v-1,\,1}(T)=\frac{1}{(kT)^3\pi r^{*2}}\int_0^{r^*}\int_0^{\infty}\int_0^{\infty}2\pi\,b\,E\,P^{s,o}_{v-1,\,1}(E_r,\,E,\,b)$$

$$\exp(-E_r/kT)\ \exp(-E/kT)\,dE_r\,\mathrm{dE}\,\mathrm{db}\quad(12)$$

In averaging over E_r, we shall replace E_r by the average energy $\bar{E}_r=\frac{1}{4}[E_r^{1/2}+(E_r+\hbar\Delta\omega)^{1/2}]^2$.

Results and Discussion

For the calculation, the spectroscopic constants were taken from the the standard tables.[26] The interaction parameter a is estimated in terms of the Lennard-Jones (L−J) constants from the equation[27] $a=\sigma_{LJ}\pi^{-1/2}[\Gamma(7/12)/\Gamma(1/12)](4\varepsilon/E^*)^{1/2}$, where $E^*=\{[7\Gamma(7/12)/\Gamma(1/12)](2\pi\mu)^{1/2}(C\Delta E\,kT/\hbar)\}^{12/19}$ and $C=\sigma_{LJ}(4\varepsilon)^{1/12}/12$. The Lennard-Jones constants[28] are $\varepsilon_{LJ}(H_2)=33.3\,k$, $\varepsilon_{LJ}(D_2)=39.3\,k$, $\varepsilon_{LJ}(HF/DF)=400\,k$, $\sigma_{LJ}(H_2)=2.915$ Å, $\sigma_{LJ}(D_2)=2.948$ Å, and $\sigma_{LJ}(HF/DF)=2.55$ Å. Using the constants given above, we find $a=0.292\ T^{-1/19}$ Å for $HF+H_2$ and $a=0.300\ T^{-1/19}$ Å for $DF+D_2$. The energy transfer probabilities in Eq. (8) and (12) is slightly dependent on the change in a. The above relation shows a slight temperature dependence of the value of a; *e.g.*, the values of the potential parameter a vary from 0.221 Å at 200 K to 0.203 Å 1000 K for $HF+H_2$ and from 0.227 Å at 200 K to 0.209 Å at 1000 K for $DF+D_2$. Furthermore, as the calculation of the energy transfer probabilities was carried out for the temperature range from 200 to 800 K where the long-lived collision theory is expected to be valid, we take $a=0.22$ Å for both $HF+H_2$ and $DF+D_2$. We choose 0.6 kcal/mol as attractive energy D from *ab initio* study by Sapes[10]. The integration in Eq. (8) and (12) is carried out numerically.

The calculated results of the $V-V$, T, $V-V$, R and the overall $V-V$ energy transfer probabilities (*i.e.*, the sum of the $V-V$, T and $V-V$, R contributions) are shown in Figures 1 to 4 for the process (a) and in Figures 5 to 8 for the process (b). As shown in Figures 1 to 4, the overall $V-V$ probabilities for the process (a) increase with the increase in temperature. This is because, when temperature increases, the long-lived collisions (*i.e.*, $V-V$, T mechanism)

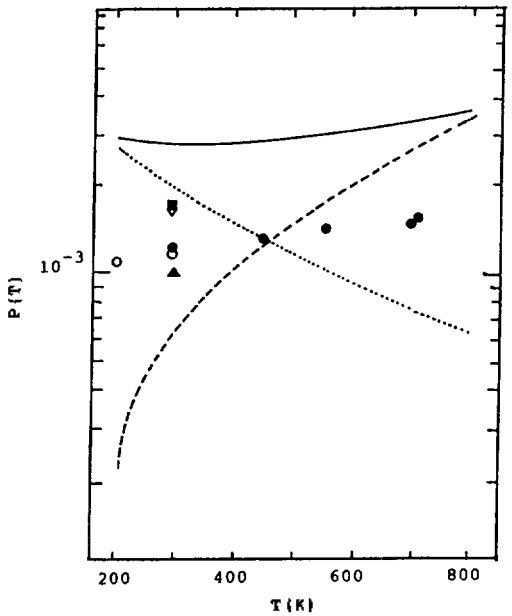

Figure 1. Vibration to vibration energy transfer probabilities for $HF(v=1)+H_2(v=0)\rightarrow HF(v=0)+H_2(v=1)$. The dotted curve represents the result of the $V-V$, T model, the broken curve the result of the $V-V$, R model, and the solid curve the sum of these two results. Experimental data: ■, Ref. 11; ▽, Ref. 12; ●, Ref. 13; ▲, Ref. 16; ○, Ref. 20.

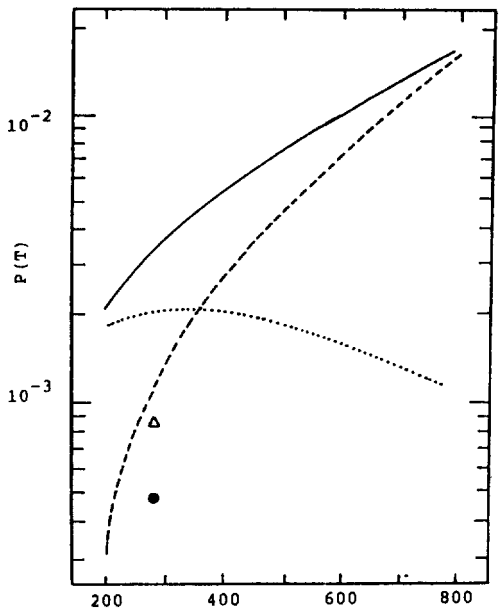

Figure 2. Vibration to vibration energy transfer probabilities for $HF(v=2)+H_2(v=0)\rightarrow HF(v=1)+H_2(v=1)$. The dotted curve represents the result of the $V-V$, T model, the broken curve the result of the $V-V$, R model, and the solid curve the sum of these two results. Experimental data: △, Ref. 16; ●, Ref. 17.

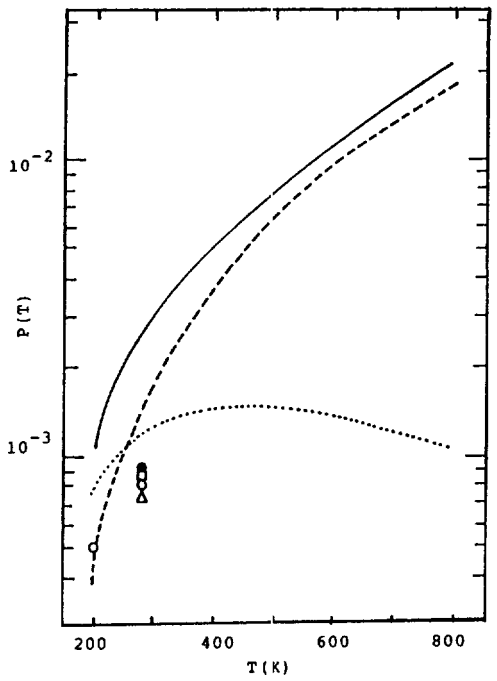

Figure 3. Vibration to vibration energy transfer probabilities for $HF(v=3)+H_2(v=0)\rightarrow HF(v=2)+H_2(v=1)$. The dotted curve represents the result of the $V-V$, T model, the broken curve the result of the $V-V$, R model, and the solid curve the sum of these two results. Experimental data: □, Ref. 16; △, Ref. 18; ○, Ref. 20; ●, Ref. 22.

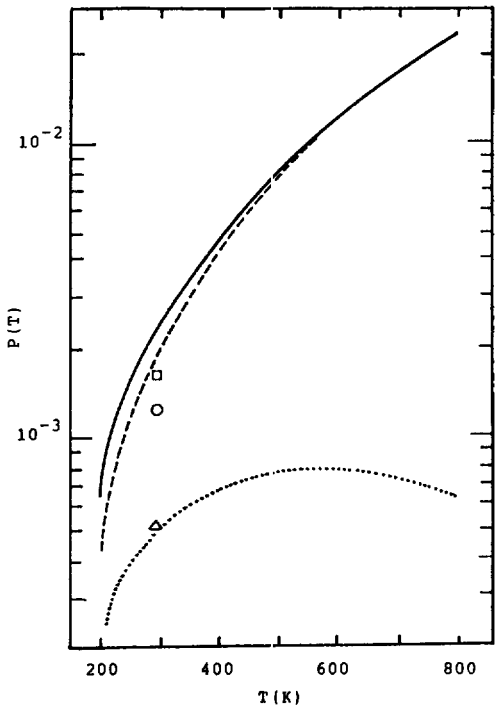

Figure 4. Vibration to vibration energy transfer probabilities for $HF(v=4)+H_2(v=0)\rightarrow HF(v=3)+H_2(v=1)$. The dotted curve represents the result of the $V-V$, T model, the broken curve the result of the $V-V$, R model and the solid curve the sum of these two results. Experimental data: △, Ref. 17; ○, Ref. 18; □, Ref. 22.

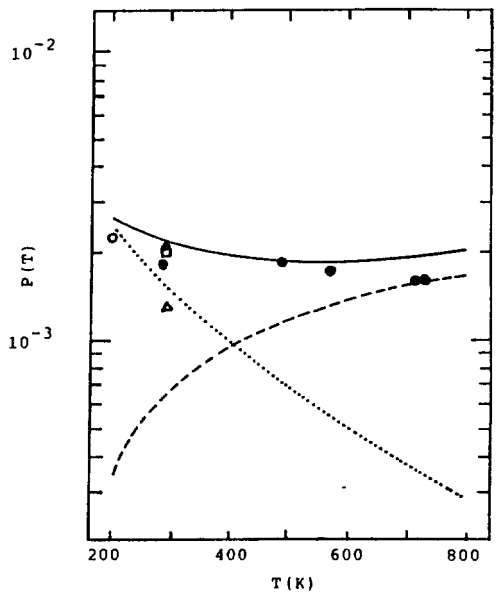

Figure 5. Vibration to vibration energy transfer probabilities for $DF(v=1)+D_2(v=0)\rightarrow DF(v=0)+D_2(v=1)$. The dotted curve represents the result of the $V-V$, T model, the broken curve the result of the $V-V$, R model, and the solid curve the sum of these two results. Experimental data: □, Ref. 12; ●, Ref. 14; ▲, Ref. 15; △, Ref. 19; ○, Ref. 21.

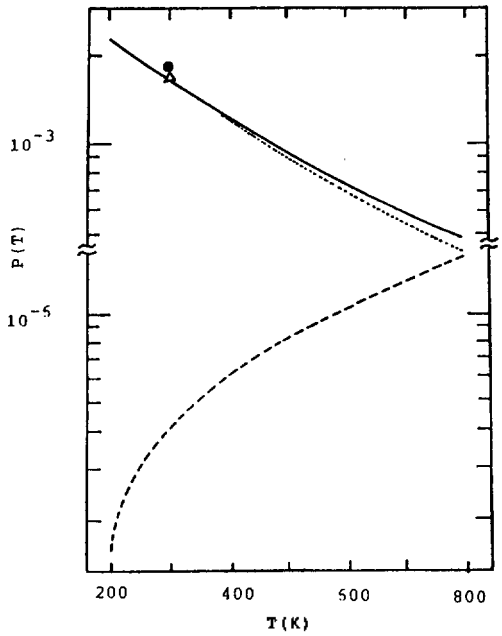

Figure 6. Vibration to vibration energy transfer probabilities for $DF(v=2)+D_2(v=0)\rightarrow DF(v=1)+D_2(v=1)$. The dotted curve represents the result of the $V-V$, T model, the broken curve the result of the $V-V$, R model, and the solid curve the sum of these two results. Experimental data: ●, Ref. 15; △, Ref. 19.

are of no longer importance, and the energy transfer mechanism by the rapid rotational motion (*i.e.*, $V-V$, R mechanism) plays an important role[29]. For the process (b) as shown in Figures 5 to 8 the overall $V-V$ probabilities, except for $n=4$, decrease with the increase in temperature and in excellent

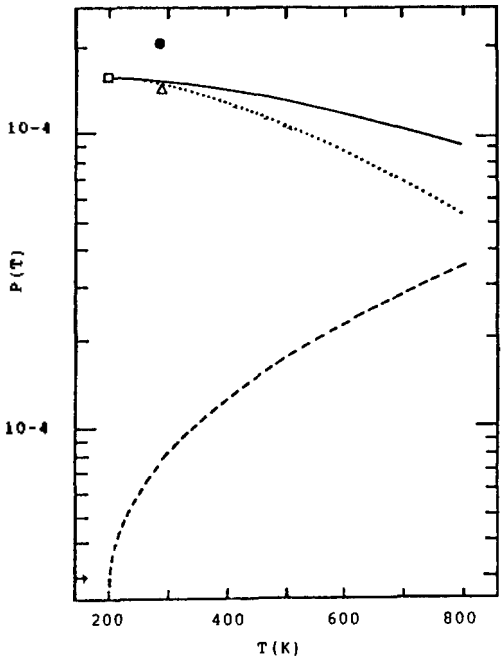

Figure 7. Vibration to vibration energy transfer probabilities for $DF(v=3)+D_2(v=0)\rightarrow DF(v=2)+D_2(v=1)$. The dotted curve represents the result of the $V-V$, T model, the broken curve the result of the $V-V$, R model, and the solid curve the sum of these two result. Experimental data: ●, Ref. 15; △, Ref. 19; □, Ref. 21.

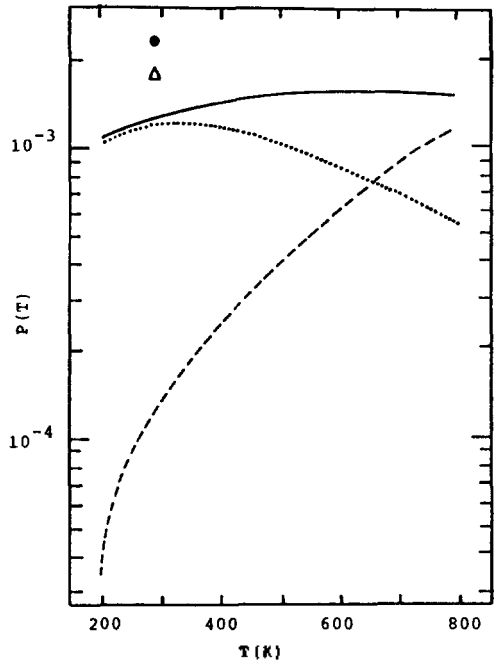

Figure 8. Vibration to vibration energy transfer probabilities for $DF(v=4)+D_2(v=0)\rightarrow DF(v=3)+D_2(v=1)$. The dotted curve represents the result of the $V-V$, T model, the broken curve the result of the $V-V$, R model, and the solid curve the sum of these two result. Experimental data: △, Ref. 15; ●, Ref. 19.

agreement with the experimental results. This fact could be explatned in terms of the energy mismatch ΔE. In this case the energy mismatch of the process (b), the magnitudes of endothermicity, is quite smaller than that of the corresponding process (a). For example, when n is 1, 2, 3, and 4, the energy mismatch, ΔE is 199, 369, 576 and 693 cm^{-1} for the process (a) and 85, 177, 268 and 360 cm^{-1} for the process (b), respectively. That is, the magnitudes of ΔE for the process (b) are almost half of those for the process (a). In general energy transfer process becomes less efficient as the amount of internal energy transferred into translational motion increases. When ΔE is large, therefore, the $V-V$, T cannot play an important role due to the increased nonresonance character. However, when ΔE is small, the $V-V$, T mechanism now becomes more important relative to the $V-V$, R. Because of this small ΔE, the overall $V-V$ probabilities for the process (b) are mainly dependent on $V-V$, T mechanism, showing the so-called negative temperature dependence.

For comparision with other experimental data, the overall $V-V$ probabilities for process (a) and process (b) at 300 K are collected in Tables 1 and 2, respectively along with other available experimental results. As can be seen in Tables and Figures, our calculated results for the process (b) agree well with those obtained experimentally, but those for the process (a) show a slightly larger values compared with the experimental results. When $n=1$ in both the collision system of $HF+H_2$ and $DF+D_2$, temperature dependence of the overall $V-V$ probabilites also agrees well with the experimental results. Thus, it is shown that our approach to predict the energy exchange probability for the process (a) and (b) is valid, at least when $n=1$. For the case of the system $HF(v=2-4)+H_2(v=0)$, the overall $V-V$ probabilites calculated show sharply positive dependence on the temperature, while the system $HF(v=1)+H_2(v=0)$ shows very weak ten-

Table 1. Vibration-to-Vibration Energy Transfer Probabilities for $HF(v=n)+H_2(v=0)\rightarrow HF(v=n-1)+H_2(v=1)$ at 300 K

$v=1$	$v=2$	$v=3$	$v=4$	Ref.
1.22×10^{-3}		$8.17\times^{-4}$		Bott and Heidner[20]
1.03×10^{-3}	9.00×10^{-4}	$8.18\times^{-4}$		Bott[16]
1.23×10^{-3}				Bott and Cohen[13]
1.74×10^{-3}				Hancock and Green[11]
1.73×10^{-3}				Hinchen[12]
	5.0×10^{-4}	3.6×10^{-4}	5.1×10^{-5}	Pool and Smith[17]
		7.52×10^{-4}	1.12×10^{-3}	Douglus and Moore[18]
		9.00×10^{-4}	1.57×10^{-3}	Jursich, Ritter and Crin[22]
2.73×10^{-3}	3.64×10^{-3}	3.05×10^{-3}	2.20×10^{-3}	This work

Table 2. Vibration-to-Vibration Energy Transfer Probabilities for $DF(v=n)+D_2(v=0)\rightarrow DF(v=n-1)+D_2(v=1)$ at 300 K

$v=1$	$v=2$	$v=3$	$v=4$	Ref.
2.02×10^{-3}	1.78×10^{-3}	1.52×10^{-3}	1.82×10^{-3}	Bott[19]
1.99×10^{-3}				Hinchen[12]
1.85×10^{-3}				Bott[14]
1.33×10^{-3}	1.85×10^{-3}	2.12×10^{-3}	2.38×10^{-3}	Kwok and Wilkins[15]
2.12×10^{-3}	1.65×10^{-3}	1.56×10^{-3}	1.34×10^{-3}	This work

dency. Also the overall $V-V$ probabilites are larger than the experimental values. However, as the available experimental data exist at only two temperatures of 200 K and 300 K, it may be too early to conclude the validity of this model.

Figures 1 to 8 also show the relative importance of the two competing energy transfer pathways, $V-V$, T and $V-V$, R in inducing the $V-V$ energy transfer. As shown in Figure 1 to 4, when $n=1$, the $V-V$, T probabilities calculated for the process (a) decrease with increase in temperature, that is, showing a negative temperature dependece, while for $n=$ 2, 3, and 4, the $V-V$, T probabilities show maximum values near 300 K, 450 K and 600 K, respectively. In Eq. (8), E is replaced by the symmetrized energy $\bar{E}=(E_i^{1/2}+E_f^{1/2})$. When the impact parameter is considered, $E_i=E(1-b^2/r^{*2})$ and $E_f=E(1-b^2/r^{*2})+\Delta E$. Also the integration range in Eq. (8) is $0\leq E\leq D^*$. Therefore, when ΔE is much smaller than D^*, the $V-V$, T energy transfer probability decreases with temperature but when ΔE is large, it goes through maximum and then, because of exponential term in Eq. (8), decreases as temperature is increased. In the present $V-V$, T calculation $n=2$, 3 and 4 for process (a) and $n=4$ for the process (b) in which the difference between D^* and ΔE is not large show maximum values. All $V-V$, R probabilities for the process (a) increase sharply with increase in temperature. Therefore, as temperature increases a major portion of the overall $V-V$ energy transfer for the process (a) occurs by $V-V$, R. On the other hand, for the processes (b) all $V-V$, T probabilities show typical negative temperature dependence and $V-V$, R probabilities show a positive dependence. For $n=1$, the overall $V-V$ transition are mainly dependent on the $V-V$, T at low temperature but occur predominantly via the $V-V$, R path with rising temperature. However, the $V-V$, R contribution to the overall process for $n=2$-3 is very small compared with that of the $V-V$, T model. The $V-V$, R contribution to overal $V-V$ process for $n=4$ is also very small at low temperature. For a large ΔE, the $V-V$, T mechanism is not expected to play an important role due to the increased endothermic character. When $n=1$, 2, 3, and 4, the $V-V$, T fractions for the process (a) are 77, 61, 44, and 21% at 300 K, respectively. That is, in the process (a), the $V-V$, R process dominates over the $V-V$, T process in the overall $V-V$ process for large v. But the $V-V$, R fractions for the process (b) are neligible except for $n=1$ at low temperature. For the process (b), ΔE is almost half of the endothermicity for the processes (a) as noted before, so the relative fractions of the $V-V$, R to the overall $V-V$ energy transfer probabilites are below 10% at 300 K, which are much smaller than the corresponding values of the processes (a). Even though the energy mismatch ΔE for the process (b) is much smaller than that for the process (a), it is an unexpected result that the $V-V$, T fractions for $n=2$-4 are over 90% considering that the attractive force between DF and D_2 is very small, that is, $D=0.6$ kcal/mol. For both the processes (a) and (b), the variation of the overall $V-V$ probabilities with the vibratioal quantum number v tends to decrease with v at low temperature, while at high temperature it tends to increase.

In summary, the overall $V-V$ energy transfer probabilites for $HF(v=n)+H_2(v=0)$ and $DF(v=n)+D_2(v=0)$ using the long-lived collision model and the vibration to vibration and rotation energy transfer model have been calculated semiclassically. Even though the collision model used in this study is very simple, it can explain the essential features of the $V-V$ energy transfer for $HF+H_2$ and $DF+D_2$.

Acknowledgement. We thank the Basic Sciences Research Institute of Inha University for financial support.

References

1. S. Ormonde, *Rev. Mod. Phys.*, **47**, 193 (1975).
2. J. F. Bott, Aerospace Report, SAMSO-TR-74-287 (1976).
3. S. R. Leone, *Chem. Ref. Data*, **11**, 953 (1982).
4. K. J. Rensberger, J. M. Robinson, and F. F. Crim, *J. Chem. Phys.*, **86**, 1340 (1987) and references therein.
5. D. Papadimitrius and B. Schramm, *J. Chem. Phys.*, **90**, 6171(1989).
6. C. S. Lee and Y. H. Kim, *J. Kor. Chem. Soc.*, **28**, 26 (1985) and references therein.
7. H. K. Shin and Y. H. Kim, *J. Chem. Phys.*, **73**, 3186 (1980).
8. C. S. Lee, Y. H. Kim, and H. K. Shin, *J. Kor. Chem. Soc.*, **28**, 361 (1984).
9. J. Ree, C. K. Sohn, C. S. Lee, and Y. H. Kim, *Bull. Korean Chem. Soc.*, **8**, 449 (1987).
10. A. Sapes, *J. Chem. Phys.*, **78**, 5733 (1983).
11. J. K. Hancock and W. H. Green, *J. Chem. Phys.*, **56**, 4515 (1972).
12. J. J. Hinchen, *J. Chem. Phys.*, **59**, 233 (1973).
13. J. F. Bott and N. Cohen, *J. Chem. Phys.*, **58**, 4539 (1973).
14. J. F. Bott, *J. Chem. Phys.*, **60**, 427 (1974).
15. M. A. Kwok and R. L. Wilkins, *J. Chem. Phys.*, **63**, 2453 (1975).
16. J. F. Bott, *J. Chem. Phys.*, **65**, 4239 (1976).
17. P. R. Poole and I. W. M. Smith, *J. Chem. Soc. Faraday Trans.*, **73**, 1434 (1977).
18. D. J. Douglas and C. B. Moore, *J. Chem. Phys.*, **70**, 1769 (1979).
19. J. F. Bott, *J. Chem. Phys.*, **70**, 4123 (1970).
20. J. F. Bott and R. F. Heidner, *J. Chem. Phys.*, **72**, 3211 (1980).

21. J. F. Bott, *J. Chem. Phys.*, **74**, 2827 (1981).
22. G. M. Jursich, D. R. Ritter, and F. F. Crim, *J. Chem. Phys.*, **80**, 4097 (1984).
23. H. K. Shin, *J. Chem. Phys.*, **78**, 795 (1983).
24. R. L. Wilkins, *J. Chem. Phys.*, **67**, 5838 (1977).
25. H. K. Shin, *J. Phys. Chem.*, **75**, 1079 (1971).
26. K. P. Huber and G. Herzberg, "Constants of Diatomic molecules." Van Nostrand Reinhold Co., New York (19 79).
27. H. K. Shin, *J. Chem. Phys.*, **41**, 2864 (1964).
28. J. O. Hirschfelder, C. F. Curties, and R. B. Bird, "Molecular Theory of Gases and Liquids," Wiley, New York (1964).
29. H. K. Shin and Y. H. Kim, *J. Chem. Phys.*, **64**, 3634 (1976).

Picosecond Photoionization Processes of N,N,N′,N′-Tetramethyl-*p*-phenylenediamine (TMPD) in Water

Minyung Lee*, Du-Jeon Jang, and Dongho Kim

Spectroscopy Laboratory, Korea Research Institute of Standards and Science, Taejeon 305-606

Sun Sook Lee and Bong Hyun Boo

Department of Chemistry, Chungnam National University, Taejeon 305-746. *Received July 24, 1991*

Photoionization processes of TMPD in H_2O and D_2O were studied, by measuring steady-state absorption, emission, fluorescence excitation spectra, and fluorescence lifetimes on picosecond time scale. The steady-state absorption spectra showed that there exists a cation-ion pair (Wurster's Blue) in H_2O and in D_2O in the electronic ground state. Temperature and excitation wavelength dependence were also studied ant the results show that the photoionization reaction in water is an activated process and the fluorescence lifetime is independent of the vibrational excess energy in the uv excitation range of 283-310 nm.

Introduction

Upon electronic excitation, TMPD is known as one of the simplest molecules undergoing one-photon ionization in polar solvents such as water, acetonitrile, and alcohols[1-4]. Recently, time-resolved nanosecond and picosecond studies have been carried out in many laboratories to elucidate dynamics of electron photoejection from TMPD in the first excited singlet state[5-9]. It seems that the photoionization process depends on the nature of solvents. For example, the fluorescence lifetimes of TMPD in alcohols are affected by solvent polarity. The lifetimes of TMPD at room temperature are 3.7, 7.3, and 7.6 ns in methanol, ethanol, and butanol, respectively[10]. Since the photoionization rate is roughly proportional to the inverse of the fluorescence lifetime, high solvent polarity facilitates the electron ejection by lowering the activation energy, which has been confirmed by temperature-dependent studies on fluorescence lifetime measurements[10].

In acetonitrile, the fluorescence lifetime of TMPD is much shorter (1.0 ns), compared with alcohols. Mataga and coworkers extensively studied the photoionization process of TMPD and analogous molecules in acetonitrile[5-7,11,12]. Based on their accumulated experimental data and recent experiments on the excittion wavelength dependence[13], they concluded that the ionization occurs from the relaxed S_1 state (fluorescence state) and the rate of the electron ejection from the vibrationally unrelaxed state depends not only on the excess energy but also on the nature of the excited vibrational modes.

The polarity of water is so strong that TMPD forms a cation-ion pair, so-called "Wurster's bule (WB)" in water even in the electronic ground state. Therefore, it is more difficult to interpret the experimental observations on ptoto-induced reaction process of TMPD in water. Richards and Thomas first studied the photoionization of TMPD in water-ethanol mixture with microsecond and nanosecond time resolution[2]. They observed that the rapid fluorescence quenching of TMPD in the mixture as the concentration of water increases. From our previous measurements on fluorescence lifetimes of TMPD in water-ethanol mixture, we suggested that the decrease of the quantum yield in the high concentration of water was due to the fast electron transfer of TMPD[10]. However, the time resolution was limited by the instrument response so that the photoionization rate were not able to be measured accurately. It should be noted that Richards and Thomas reported that TMPD did not fluoresce in aqueous solution. However, our steady state emission and fluorescence lifetime data show that TMPD does fluoresce in H_2O and in D_2O.

In this work, we study the photoionization dynamics of TMPD in H_2O and D_2O in picosecond time scale. The lifetimes of TMPD in those solvents were measured with a 10 ps temporal resolution. The activation energy and the Arrehenius factor were measured by obtaining fluorescence lifeti-